Convert Acoustic Resonances to Orbital Angular Momentum

Xue Jiang,[1] Yong Li,[2] Bin Liang,[1,*] Jian-chun Cheng,[1,†] and Likun Zhang[3,‡]

[1]*Collaborative Innovation Center of Advanced Microstructures and Key Laboratory of Modern Acoustics, MOE, Institute of Acoustics, Department of Physics, Nanjing University, Nanjing 210093, People's Republic of China*

[2]*CNRS, Institut Jean Lamour, Vandœuvre-lès-Nancy F-54506, France and Université de Lorraine, Institut Jean Lamour, Boulevard des Aiguillettes, BP: 70239, Vandœuvre-lès-Nancy 54506, France*

[3]*Department of Physics and Center for Nonlinear Dynamics, University of Texas at Austin, Austin, Texas 78712, USA*

(Received 16 March 2016; published 12 July 2016)

We use acoustic resonances in a planar layer of half-wavelength thickness to twist wave vectors of an in-coming plane wave into a spiral phase dislocation of an outgoing vortex beam with orbital angular momentum (OAM). The mechanism is numerically and experimentally demonstrated by producing an airborne Bessel-like vortex beam. Our acoustic resonance-based OAM production differs from existing means for OAM production by enormous phased spiral sources or by elaborate spiral profiles. Our study can advance the capability of generating phase dislocated wave fields for further applications of acoustic OAM.

DOI: 10.1103/PhysRevLett.117.034301

Wave fields with spiral phase dislocations [1] carry orbital angular momentum (OAM) such as for sound fields [2], optical waves [3], and electron beams [4]. A spiral phase $\exp(im\theta)$ linearly proportional to the azimuth angle θ is associated with a null field at the core. The carried OAM is discretized with the integer m (topological charge or order of the beam) to have an OAM-to-energy ratio m/ω (where ω is the radian frequency) for both quantum [3,4] and classical waves [5,6]. Transfer of the OAM to matter produces a torque associated with the transfer of wave energy such as in optical [7–9] and acoustic waves [5,10–14].

Acoustic waves with spiral phases and OAM with useful properties (e.g., Refs. [15–19]) were generated by phased spiral sources or physically spiral sources. A phased spiral source consists of an array of individually addressed transducers excited with appropriate screw phases to produce the expected phase profile in acoustic vortex beams [2,20] or vortices of surface waves [21,22]. A physically spiral source is a passive structure with screw dislocated profiles to produce phase profiles in wave fields, e.g., a helical substrate underneath a ferroelectret film for airborne ultrasonic vortex generation [23], an absorbing surface with a helix dimension for the optoacoustic generation of a helical ultrasonic beam [24], a spiral-shaped object (spiral phase plate) for chiral scattering [25], and spiral gratings for diffracting waves into stable vortex beams [26].

The general principle for producing the spiral phase (denoted by ϕ_{out}) can be written as

$$\phi_{\text{out}}(\theta) = \phi_{\text{in}} + k^{\text{eff}} l, \tag{1}$$

where the dependence of ϕ_{out} on the azimuth angle θ was produced via a θ-dependent phase ϕ_{in} in phased spiral sources or via a θ-dependent propagation distance l through physically spiral sources.

The OAM production in this study does not have to rely on the θ dependence in either the phase ϕ_{in} or the propagation distance l in Eq. (1). Instead we produce a θ-dependent effective wave number k^{eff}. The mechanism is that, regardless of no θ dependence in the phase ϕ_{in} of an axisymmetric in-coming wave and in the propagation distance l of a planar layer [Fig. 1], acoustic resonances are excited in the layer to eventually produce the desired wave number k^{eff} for twisting the wave vectors into a phase dislocation of a vortex beam with OAM. We numerically model and experimentally demonstrate this mechanism by generating a Bessel-like vortex beam.

Model.—We construct the planar layer as an assembly of eight fanlike sections of resonators over the whole azimuth [Fig. 2(a)]. This number of sections gives a reasonably good resolution for generating a vortex beam with a topological charge $m = 1$, as will be demonstrated via both numerical simulations and experimental

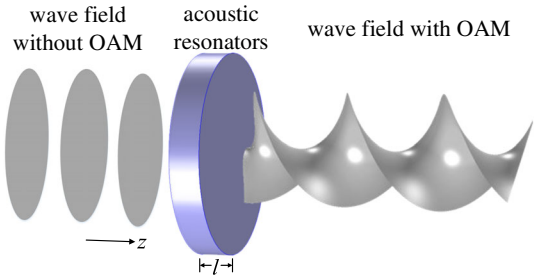

FIG. 1. Illustration of a resonant planar layer (blue) converting an in-coming axisymmetric wave without orbital angular momentum (OAM) to an outgoing beam with a helical wave front carrying OAM (wave fronts are shown in gray).

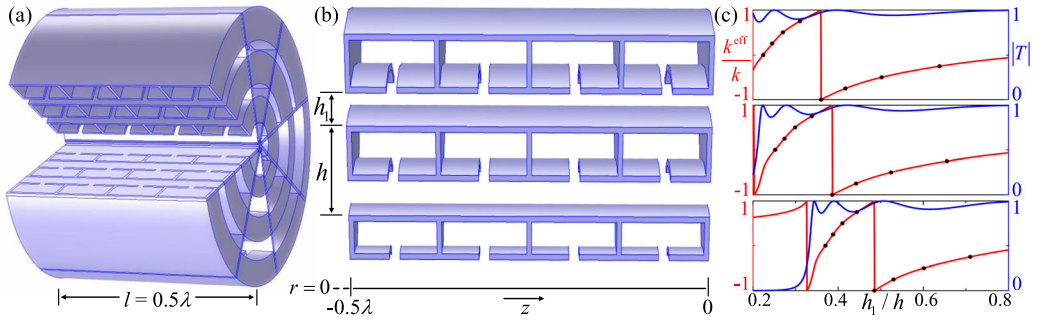

FIG. 2. (a) Schematic of the assembled layer consisting of eight fanlike sections of resonators. (b) An individual section consisting of three rows of resonators in the radial r direction (the radial resolution $h = 0.1\lambda$ with λ being the sound wavelength), sided by pipes of varying height h_1 to produce the needed effective wave number [cf. Eq. (1)]; the thickness of the walls is 0.01λ. (c) The effective wave number k^{eff} (red; normalized by $k = 2\pi/\lambda$) and transmission coefficient $|T|$ (blue) as functions of the height ratio h_1/h simulated for the three rows in (b), where in each case the eight black dots are parameters selected for the eight sections in (a) with equally discrete wave numbers to generate a first-order vortex beam. The averaged transmission efficiency of these 8×3 elements is $|T| = 95.1\% \pm 3.8\%$.

measurements. For generating higher-order vortex beams, the number of sections in the resonant layer can be increased for a finer resolution.

Each individual section [Fig. 2(b)] is configured to be composed of three rows of resonators in the radius (more rows can be employed for a larger radius). Each row consists of four Helmholtz cavities and a straight pipe [27]: (i) the series connection of four cavities acting as lumped elements is for a fully flexible manipulation of wave numbers k^{eff} (or phases), (ii) the combination of cavities and pipes provides hybrid resonances that overcome the impedance mismatch between the resonators and the surrounding air for a high transmission, and (iii) the layer is optimized to have a propagation distance $l = 0.5\lambda$, a value that is small enough to maintain hybrid resonances, but large enough for negligible viscous effects (with the width of each cavity's neck in air fixed at 0.025λ) and for manipulating the wave number k^{eff} over a fully desired range (a reasonably good performance can still be obtained with $l \gtrsim 0.4\lambda$; cf. Fig. 3 in Ref. [27]).

We use the resonant layer to produce the desired spiral phases and OAM by manipulating k^{eff} for an azimuthal dependence via tuning the height of the cavities into an azimuthal dependence. The k^{eff} values are modulated for the eight sections individually, denoted by $k_j^{\text{eff}} (j = 1, 2, \ldots, 8)$. Consider generating a first-order $m = 1$ vortex beam; the k_j^{eff} values selected for the eight sections cover the whole range from $-k$ to k with a step of $k/4$ (where $k = 2\pi/\lambda$ is the wave number in the surrounding medium). If the three rows of resonators have an identical transmission, the outgoing normalized field from an individual segment is approximated by

$$p|_{z=0} = \exp(ik_j^{\text{eff}} l - i\omega t) \quad \text{for } (j-1)\pi/4 < \theta < j\pi/4. \tag{2}$$

The outgoing wave propagates in a rigid cylindrical waveguide of radius a as for generating a vortex beam of a Bessel-like profile. The wave can be represented as a sum of cylindrical Bessel modes:

$$p = \sum_m \sum_n A_{m,n} J_m(k_{m,n} r) \exp(ik_z z + im\theta - i\omega t), \tag{3}$$

where $A_{m,n}$ is the modal amplitude, $J_m(k_{m,n}r)$ is the m-order Bessel function, $k_{m,n}$ is the nth positive root of the equation $\partial J_m(k_{m,n}r)/\partial(k_{m,n}r)|_{r=a} = 0$, and the axial wave number is $k_z = \sqrt{k^2 - k_{m,n}^2}$. We restrict the $(m, n) = (1, 1)$ mode as the only propagating vortex mode in the waveguide by choosing k to be higher than the critical wave number of the (1,1) mode (i.e., $k_{1,1}$) but lower than that of the (1,2) mode (i.e., $k_{1,2}$). Given the condition at $z = 0$ in Eq. (2), the normalized propagating field would be

$$p = J_1(k_{1,1} r) \exp(ik_z z + i\theta - i\omega t), \tag{4}$$

which is exactly a first-order Bessel-like vortex beam (topological charge $m = 1$) that carries OAM.

Simulations and measurements.—Now we simulate the conversion of the acoustic resonances to OAM with a finite element method based on COMSOL MULTIPHYSICS software (with the pressure acoustic interface [28]). The simulations resemble the experimental setup of an in-coming wave at 2287 Hz (with an airborne wavelength of 15 cm), simulated as a plane wave to propagate along an air-filled cylindrical waveguide of 5-cm radius and transmit through a coaxial resonant layer of 7.5-cm thickness. The airborne sound wave number $k = 41.9$ rad/s is in between the values of $k_{1,1} = 36.8$ rad/s and $k_{1,2} = 106.4$ rad/s of the waveguide, satisfying the criteria stated in the aforementioned model analysis. Solid materials (used in the experiments) for the waveguide (PMMA) and for the layer (UV resin) are treated as acoustically rigid in the simulations because of the strong contrast of acoustic impedance between these materials and air [29].

Simulations individually for the three rows in Fig. 2(b) (via two-dimensional axisymmetric simulations) indicate an almost unity transmission $|T|$ over a wide range of height ratio h_1/h [Fig. 2(c), blue curves], guaranteeing the efficient conversion of acoustic resonances to OAM. The effective wave number k^{eff}, calculated from $\arg(T)/l$, exhibits the required coverage of the full $2k$ range [Fig. 2(c), red curves], where the eight dots give the eight discrete k_j^{eff} values for the eight sections in Fig. 2(a). Their transmissions have an average of 95.1% ±3.8%.

The simulated transmission through the whole layer (via three-dimensional simulations in the air-filled waveguide) exhibits an expected twisted wave front with a screw dislocation along the propagation axis [Fig. 3(a)]. The distribution of phases and sound amplitudes at the four cross sections [Fig. 3(b)] illustrates a transition from the near to the far field. The transition point would be around $a^2/\lambda = 0.11\lambda$, estimated from the radiation of a circular piston [30]. The distortion in both the phases and amplitudes is obvious at the cross section $z = 0.01\lambda$ [left hand side panels in Fig. 3(b)], while at the rest of three cross sections $z \geq 0.11\lambda$ the phase regularly jumps 2π over one annular loop, revealing the expected topological charge $m = 1$. Another representative characteristic of the Bessel-like vortex—the null pressure amplitude at the core—is also clearly shown in Fig. 3(b) (bottom), where a small asymmetry over the azimuth is due to the small differences of the transmission $|T|$ among the resonators [Fig. 2(c)]. The overall transmission efficiency through the layer is 93.8% when calculated from the square root of the outgoing to in-coming sound power ratio.

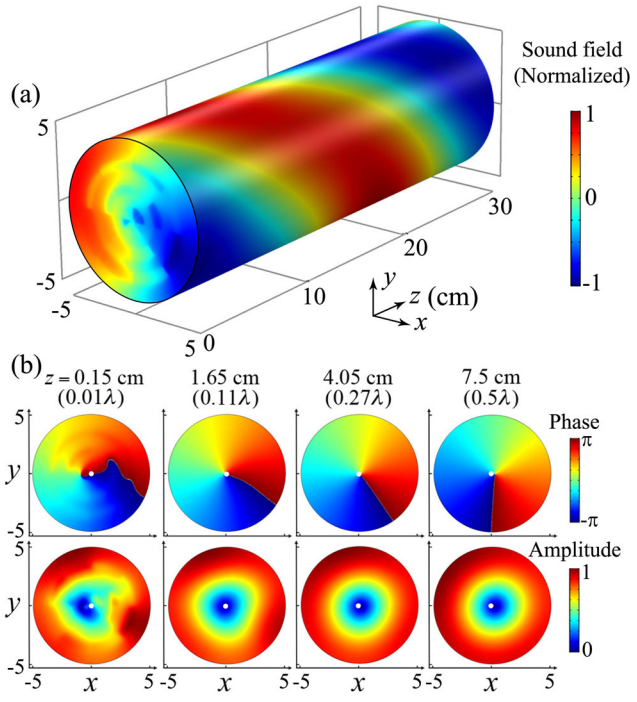

FIG. 3. Numerical simulations. (a) Airborne sound pressure field on the outgoing surface of the planar layer (located at $-0.5\lambda \leq z \leq 0$) and the inner surface of a cylindrical waveguide of 5-cm radius. (b) Phase (top) and amplitude (bottom) of the field at four cross sections, illustrating the transition from the near to the far field, where the geometric centers of the cross sections are denoted by the white dots. The simulations are for sound of a frequency 2287 Hz ($\lambda = 15$ cm in air).

Experiments to verify and demonstrate the OAM production are conducted in a 300-cm long waveguide and using a layer fabricated via 3D printing technology [Fig. 4(a) [31]]. A monochromatic sound wave, excited by a loudspeaker (4-in. diameter) facing into the waveguide at one end, propagates as a plane wave through the waveguide and illuminates the layer placed at the middle of the waveguide. The transmitted sound is absorbed by sound absorbing foam at the other end of the waveguide. A three-dimensional sound field scan is conducted by employing two microphones (1/4-in., Brüel & Kæjr type-4961) with a mobile one scanning the outgoing field with OAM and a fixed one detecting the in-coming wave as a reference signal. The phase and amplitude of the sound in each scan point are retrieved from cross spectrum of the two signals.

The measured phase distributions at the far-field cross sections $z = 0.27\lambda$ and 0.5λ [Fig. 4(b)] recover the corresponding simulated results in a good shape [Fig. 3(b)]. The phase profile is measured (via cross correlation) to rotate an angle of 0.217π rad between these two cross sections, revealing an axial wave number $k_z = 19.8$ rad/m (given the known propagation distance of 0.23λ in between), verifying a value of $k_z = \sqrt{k^2 - k_{m,n}^2} = 20$ rad/m calculated from the known frequency and cylinder geometry.

The corresponding sound amplitude measured at the two far-field cross sections is shown in Fig. 4(c) for a direct comparison with the simulated results and theoretical profiles $J_1(k_{1,1}r)$ [cf. Eq. (3)]. The results show the primary characteristics of the $m = 1$ Bessel-like vortex in the measured amplitude. The transmission (square root of the outgoing to in-coming sound power ratio) is measured to be 88.4% [32], verifying the high efficiency and the effectiveness of the proposed scheme in converting acoustic resonances to OAM.

The underlying mechanism on manipulating k^{eff} allows for adjusting the resonant frequencies and selecting the propagating mode via tailoring the structural parameters of the resonators. A proper frequency range ensures the conversion to the desired mode, chosen as the (1,1) mode in this study, while the other modes completely fall in the evanescent regime and are trapped in the near field.

Discussions.—We have used a resonant planar layer to produce a new mechanism for generating acoustic beams with OAM. The performance of the mechanism was demonstrated by employing the resonant layer to produce OAM in a first-order airborne vortex beam with a smooth spiral phase and with a Bessel-like profile. In comparison

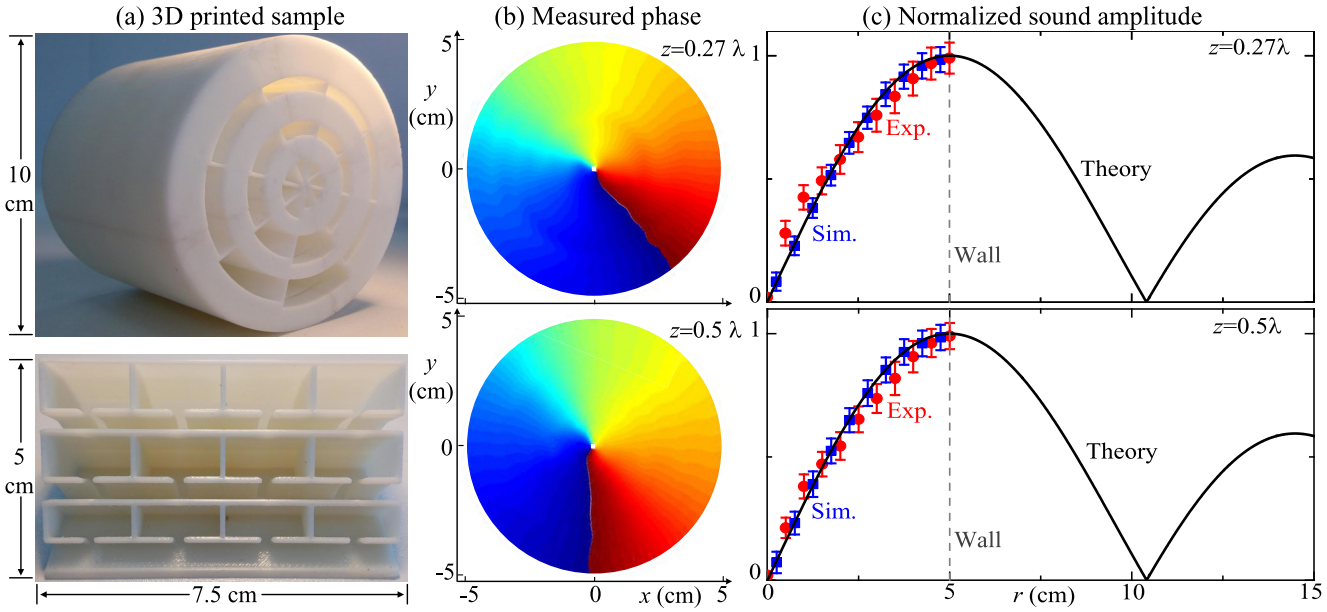

FIG. 4. Experiments. (a) The assembled sample (top) and its individual section (bottom), fabricated by 3D printing technology with a UV resin, for generating a first-order Bessel-like vortex beam in the experiments. (b) Phase distributions measured at $z = 0.27\lambda$ (top) and 0.5λ (bottom). (c) The measurements of the sound pressure amplitudes (red) as functions of radius r at the same z as in (b) are compared with numerical simulations (blue) and theoretical Bessel profiles (black). The measurements are taken at every $\pi/9$ in the azimuthal and every 0.5 cm in the radial direction. The measurements and simulations are shown in (c) as an average (dots) and an uncertainty (error bars) over the azimuthal direction. The measured transmission at these two cross sections is 88.4%.

with existing ways for OAM production by phased spiral sources that need sophisticated electronic control and by physically spiral sources that need screw profiles and may also have a bulky size, our acoustic resonance-based OAM production via manipulating effective wave numbers k^{eff} bears the advantages of high efficiency, compact size, and planar profile.

The conversion of OAM from the fundamental phenomena of acoustic resonances opens an avenue for producing acoustic vortex beams with OAM and could promote practical applications for screw wave fields. Given that the resonant planar layer employed here has a small radius, the generated vortex beam would have a strong divergence, but that divergence does not occur here for propagation in a waveguide. A layer with a larger radius though, with an increased number of resonators in both the radial and azimuthal directions, can be employed to generate a less diverging beam in free space for applications in long range alignment [2], information transmission [33], etc. The larger layer can even be used to generate a focused vortex beam provided that both k^{eff} and the transmission $|T|$ have a desired dependence on both the azimuth and radius by properly selecting the parameters of the resonators [Fig. 2(c)].

We may in principle extend the present mechanism of producing OAM via the acoustic resonance-based manipulation of the effective wave number k^{eff} to underwater propagation, but that environment requires alternative materials for a sufficient contrast of the impedance with that of water or alternative media for resonances in water (e.g., soft media [34]). The hybrid resonances used here for producing acoustic OAM overcomes the lack of classical counterpart of plasmonic resonances used for generating optical vortices [35].

X. J., B. L, and J-c. C. acknowledge support from the National Basic Research Program of China (973 Program; Grants No. 2011CB707900 and No. 2012CB921504), the Natural Science Foundation of China (Grants No. 11174138, No. 11174139, No. 11222442, and No. 81127901), NCET-12-0254, and a project funded by the Priority Academic Program Development of Jiangsu Higher Education Institutions. Y. L. acknowledges discussions with Dr. Badreddine Assouar. L. Z. acknowledges support from ONR.

X. J. and Y. L. contributed equally to the Letter.

*liangbin@nju.edu.cn
†jccheng@nju.edu.cn
‡likun.zhang.11@gmail.com

[1] J. F. Nye and M. V. Berry, Dislocations in wave trains, Proc. R. Soc. A **336**, 165 (1974).

[2] B. T. Hefner and P. L. Marston, An acoustical helicoidal wave transducer with applications for the alignment of ultrasonic and underwater systems, J. Acoust. Soc. Am. **106**, 3313 (1999).

[3] L. Allen, M. W. Beijersbergen, R. J. C. Spreeuw, and J. P. Woerdman, Orbital angular momentum of light and the transformation of laguerre-gaussian laser modes, Phys. Rev. A **45**, 8185 (1992).
[4] B. J. McMorran, A. Agrawal, I. M. Anderson, and A. A. Herzing, Electron vortex beams with high quanta of orbital angular momentum, Science **331**, 192 (2011).
[5] L. K. Zhang and P. L. Marston, Angular momentum flux of nonparaxial acoustic vortex beams and torques on axisymmetric objects, Phys. Rev. E **84**, 065601 (2011).
[6] C. E. M. Demore, Z. Yang, A. Volovick, S. Cochran, M. P. MacDonald, and G. C. Spalding, Mechanical evidence of the orbital angular momentum to energy ratio of vortex beams, Phys. Rev. Lett. **108**, 194301 (2012).
[7] H. He, M. E. J. Friese, N. R. Heckenberg, and H. Rubinsztein-Dunlop, Direct observation of transfer of angular momentum to absorptive particles from a laser beam with a phase singularity, Phys. Rev. Lett. **75**, 826 (1995).
[8] V. Garcés-Chávez, D. McGloin, M. J. Padgett, W. Dultz, H. Schmitzer, and K. Dholakia, Observation of the transfer of the local angular momentum density of a multiringed light beam to an optically trapped particle, Phys. Rev. Lett. **91**, 093602 (2003).
[9] C. M. Herne, K. M. Capuzzi, E. Sobel, and R. T. Kropas, Rotation of large asymmetrical absorbing objects by Laguerre-Gauss beams, Opt. Lett. **40**, 4026 (2015).
[10] L. K. Zhang and P. L. Marston, Acoustic radiation torque and the conservation of angular momentum (L), J. Acoust. Soc. Am. **129**, 1679 (2011).
[11] L. K. Zhang and P. L. Marston, Acoustic radiation torque on small objects in viscous fluids and connection with viscous dissipation, J. Acoust. Soc. Am. **136**, 2917 (2014).
[12] K. Volke-Sepúlveda, A. O. Santillán, and R. R. Boullosa, Transfer of angular momentum to matter from acoustical vortices in free space, Phys. Rev. Lett. **100**, 024302 (2008).
[13] A. Anhäuser, R. Wunenburger, and E. Brasselet, Acoustic rotational manipulation using orbital angular momentum transfer, Phys. Rev. Lett. **109**, 034301 (2012).
[14] Z. Y. Hong, J. Zhang, and B. W. Drinkwater, Observation of orbital angular momentum transfer from Bessel-shaped acoustic vortices to diphasic liquid-microparticle mixtures, Phys. Rev. Lett. **114**, 214301 (2015).
[15] J.-L. Thomas and R. Marchiano, Pseudo angular momentum and topological charge conservation for nonlinear acoustical vortices, Phys. Rev. Lett. **91**, 244302 (2003).
[16] K. D. Skeldon, C. Wilson, M. Edgar, and M. J. Padgett, An acoustic spanner and its associated rotational doppler shift, New J. Phys. **10**, 013018 (2008).
[17] S. T. Kang and C. K. Yeh, Potential-well model in acoustic tweezers, IEEE Trans. Ultrason. Ferroelectr. Freq. Control **57**, 1451 (2010).
[18] B. T. Hefner and B. R. Dzikowicz, A spiral wave front beacon for underwater navigation: Basic concept and modeling, J. Acoust. Soc. Am. **129**, 3630 (2011).
[19] D. Baresch, J.-L. Thomas, and R. Marchiano, Observation of a single-beam gradient force acoustical trap for elastic particles: Acoustical tweezers, Phys. Rev. Lett. **116**, 024301 (2016).
[20] R. Marchiano and J.-L. Thomas, Synthesis and analysis of linear and nonlinear acoustical vortices, Phys. Rev. E **71**, 066616 (2005).
[21] A. Riaud, J.-L. Thomas, M. Baudoin, and O. Bou Matar, Taming the degeneration of bessel beams at an anisotropic-isotropic interface: Toward three-dimensional control of confined vortical waves, Phys. Rev. E **92**, 063201 (2015).
[22] A. Riaud, J.-L. Thomas, E. Charron, A. Bussonniére, O. Bou Matar, and M. Baudoin, Anisotropic swirling surface acoustic waves from inverse filtering for on-chip generation of acoustic vortices, Phys. Rev. Applied **4**, 034004 (2015).
[23] J. L. Ealo, J. C. Prieto, and F. Seco, Airborne ultrasonic vortex generation using flexible ferroelectrets, IEEE Trans. Ultrason. Ferroelectr. Freq. Control **58**, 1651 (2011).
[24] S. Gspan, A. Meyer, S. Bernet, and M. Ritsch-Marte, Optoacoustic generation of a helicoidal ultrasonic beam, J. Acoust. Soc. Am. **115**, 1142 (2004).
[25] R. Wunenburger, J. I. V. Lozano, and E. Brasselet, Acoustic orbital angular momentum transfer to matter by chiral scattering, New J. Phys. **17**, 103022 (2015).
[26] X. Jiang, J. J. Zhao, S. L. Liu, B. Liang, X. Zou, J. Yang, C. Qiu, and J. C. Cheng, Broadband and stable acoustic vortex emitter with multi-arm coiling slits, Appl. Phys. Lett. **108**, 203501 (2016); N. Jiménez *et al.*, Formation of high-order acoustic Bessel beams by spiral diffraction gratings, arXiv: 1604.08353v1.
[27] Y. Li, X. Jiang, B. Liang, J.-c. Cheng, and L. K. Zhang, Metascreen-based acoustic passive phased array, Phys. Rev. Applied **4**, 024003 (2015).
[28] *Acoustics Module User's Guide*, COMSOL MULTIPHYSICS ® v.5.2, (COMSOL AB, Stockholm, Sweden, 2015).
[29] The density and sound speed of the PMMA for the waveguide are 1220 kg/m^3 and 3000 m/s. For the UV resin for the layer they are 1400 kg/m^3 and 1950 m/s. In contrast, they are 1.21 kg/m^3 and 343 m/s for air.
[30] L. E. Kinsler, A. R. Frey, A. B. Coppens, and J. V. Sanders, *Fundermentals of Acoustics* (John Wiley & Sons, New York, 2000).
[31] For the sake of convenient assemble and good sealing between the layer and waveguide, the fabricated sample has an addition of a central cylinder of 2-mm radius and an annulus of 3-mm thickness on the periphery.
[32] The measured transmission is lower by a small percentage than the simulated 93.8%, due to viscous dissipation in the measurements.
[33] R. Marchiano and J.-L. Thomas, Doing arithmetic with nonlinear acoustic vortices, Phys. Rev. Lett. **101**, 064301 (2008).
[34] T. Brunet, A. Merlin, B. Mascaro, K. Zimny, J. Leng, O. Poncelet, C. Aristégui, and O. Mondain-Monval, Soft 3D acoustic metamaterial with negative index, Nat. Mater. **14**, 384 (2015).
[35] N. Yu, P. Genevet, M. A. Kats, F. Aieta, J.-P. Tetienne, F. Capasso, and Z. Gaburro, Light propagation with phase discontinuities: Generalized laws of reflection and refraction, Science **334**, 333 (2011).